Asnaghi *et al. Applied Network Science* (2026) 11:24
https://doi.org/10.1007/s41109-026-00773-8

Applied Network Science

RESEARCH Open Access

A network analysis to identify possible alterations among different physiological systems induced by head down tilt bed rest

Riccardo Asnaghi[1*], Gabriel Dias Rodrigues[2], Angelica Carandina[2,3], Eleonora Tobaldini[2,3], Nicola Montano[2,3] and Manuela Ferrario[1,4]

*Correspondence:
Riccardo Asnaghi
riccardo.asnaghi@polimi.it
[1]Department of Electronics, Information, and Bioengineering (DEIB), Politecnico di Milano, P.zza L. Da Vinci, 32, 20133 Milano, MI, Italy
[2]Department of Clinical Sciences and Community Health, Dipartimento di Eccellenza 2023-2027, Università degli Studi di Milano, Via Festa del Perdono, 7, 20122 Milano, MI, Italy
[3]Department of Internal Medicine, Fondazione IRCCS Ca' Granda - Ospedale Maggiore Policlinico, Via F. Sforza, 35, 20122 Milano, MI, Italy
[4]Fondazione IRCCS Ca' Granda - Ospedale Maggiore Policlinico, Via F. Sforza, 35, 20122 Milano, MI, Italy

Abstract

Space flight introduces unique stressors, challenging the body's homeostasis. Ground-based simulations, like the − 6° head-down tilt test (HDT), help study these effects. While studies have explored the impact of space flight, they often employ limited analysis, overlooking the interconnected nature of the body's systems. This study investigates the feasibility of employing network analysis on data derived from a retrospective collection of head-down tilt bedrest experiments provided by the European Space Agency (ESA), identifying potential links among various physiological systems that may serve as novel targets for possible countermeasures. The ESA's data from HDT bed rest experiments, involving 60 subjects aged 20–46, were used. The studies included bedrest durations of 5, 21, or 60 days, with various countermeasures. Data from the BRAG study was excluded due to its short duration. Measures from control groups in the remaining studies were analyzed, including serum and urinary markers, aerobic fitness, cardiovascular responses, hematocrit levels, muscle performance, neuro-vestibular function, body composition, and daily weight. Two networks, representing baseline and post-bedrest evaluations, were constructed using Spearman partial correlation, correcting for HDT duration, number of trials, and BMI. Network topology was described using clustering coefficient, efficiency, and centrality metrics. Community detection was performed with the Louvain method, and results were compared to null models. The networks, consisting of 59 nodes each, exhibited distinct components, with some segregation of the baroreflex sensitivity indeces, as confirmed by the increased number of communities detected, as expected due to the cardiovascular deconditioning induced by gravitational unloading. Notably, cardiovascular features, particularly those associated with the autonomic nervous system (ANS), and bone markers were central in the networks. In particular, indices related to the parasympathetic branch show a predominant role in the network over the sympathetic counterpart, probably associated with anatomical aspects, and the complexity measures that provide information about the nonlinear balance in the ANS. Furthermore, bone markers seem to be influenced not only by fitness and other musculoskeletal features but also by neurovestibular and ANS factors. This influence is likely due to the activation of the sympathetic β pathway,

Springer

suggesting that the ANS represents a key potential therapeutic target for alleviating the negative effects of spaceflight and prolonged bed rest.

Keywords Bed rest, Microgravity, Cardiovascular system, Autonomic nervous system

Introduction

Space flight missions introduce an entirely new exposome encompassing a variety of factors. The body's homeostasis, i.e., the ability to adapt to new stressors, faces significant challenges during these missions. Numerous studies, particularly those involving crews on the International Space Station, have examined the physiological changes that occur during space flights (Vernice et al. 2020). The cardiovascular system is greatly affected; arrhythmias and cardiac remodeling, for example, are commonly reported. Accelerated bone remodeling, metabolic changes, and depressive symptoms have also been observed. Notably, these changes may persist even after space flight crews return to Earth (Vernikos 1996).

The long-term consequences of microgravity and the space environment are difficult to investigate due to the limited number of possible subjects who can be enrolled in this type of study. For this reason, ground-based simulation represents a good compromise. The -6° head down tilt test (HDT) bed rest is a common method for simulating the effects of microgravity on the human body. When lying on a bed tilted 6 degrees, with the head lower than the feet, the body fluids shift towards the upper body, and the gravitational load on the locomotor and postural systems becomes negligible (Gunga et al. 2016). Prolonged bed rest is known to lead to the so-called cardiovascular deconditioning, characterized by an increased resting heart rate, decreased cardiac reserve, and orthostatic intolerance. This condition can affect the body's ability to respond to sudden changes in blood pressure after periods of inactivity, such as getting up from bed (Vernice et al. 2020).

The majority of studies on microgravity rely on univariate or multivariate analyses of selected biological features, for example, bone density markers. The interactions among different organs and systems are complex and not yet fully elucidated in this context. Therefore, a more holistic approach is necessary to disentangle the multi-system physiological adaptations triggered by orthostatic stimuli removal (Ruyters et al. 2021). Understanding these mechanisms is crucial to tailor personalized countermeasures to prevent potentially life-threatening events and ensure the safety and well-being of astronauts on long-duration missions.

An emerging approach is network physiology, which employs network analysis methods to examine interconnected systems by investigating the relationships between various entities and their connections. This approach serves as a robust tool for understanding the structure, dynamics, and influences within diverse networks. It has already been applied in fields such as sleep research (Bashan et al. 2012), neuroscience (Váša and Mišić 2022), and omics (Klimek et al. 2016; Morabito et al. 2025), providing a theoretical framework for characterizing interactions within biological data. Additionally, it assists in identifying potential modifications in these interactions across different systems, particularly in the context of pathology or specific health conditions. However, the existing literature, especially concerning bed rest studies, often lacks the application of methods

that could provide a more comprehensive evaluation, taking into account the cross-talk among physiological systems.

Therefore, this study explores the feasibility of utilizing network analysis on data obtained from a retrospective collection of HDT bed rest experiments provided by the European Space Agency (ESA). The goal is to uncover connections among various physiological systems altered by the HDT condition, which may reveal novel targets for therapeutic interventions.

Materials and methods

Dataset

The European Space Agency (ESA) campaign named "Retrospective Analysis of Bedrest Core Data: a SciSpacE Announcement of Opportunity" provides a retrospective collection of -6° HDT bed rest campaigns collected between 2010 and 2019. The dataset comprises information from 107 subjects aged between 20 and 46 years. Each campaign followed comparable experimental protocols, continuous medical supervision, controlled diet and fluid intake, and a fixed daily schedule. Environmental factors such as temperature, lighting, and activity levels were carefully regulated to ensure reproducibility across studies. This approach minimizes potential inter-protocol variability, ensuring that the observed differences reflect physiological adaptations rather than experimental heterogeneity. It includes several measures and data about the bone system, cardiovascular system, anthropometric data, muscular performance, neuro-vestibular function, nutrition, ophthalmologic examinations, and psychological questionnaires from seven different studies: AGBRESA (Frett et al. 2020), BRAG (Rittweger et al. 2015), Cocktail (Arc-Chagnaud et al. 2020), MEP (Blottner et al. 2014), MNX (Guinet et al. 2020), NUC (Heer et al. 2014), and RSL (Kramer et al. 2017). These studies involved participants undergoing 5, 21, or 60 days of bed rest; they varied in terms of their design, and a number of countermeasures were implemented, including artificial gravity, reactive jumps, and nutritional supplements. Some of these studies (BRAG, MEP, MNX, NUC) used a crossover design, while the others use a parallel design. Data from the BRAG study were excluded from our analysis because participants only underwent five days of bed rest. This was deemed insufficient to induce the same degree of cardiovascular deconditioning observed in studies involving longer periods of bed rest. Longer bed rest can also produce cardiac remodeling, e.g., a chronic decrease in left ventricular mass (Hoffmann et al. 2022). For the successive analyses, we considered only the subjects who didn't undergo any countermeasures, i.e., the control group of the included studies, and who did not drop out of the study. The total number of subjects considered in this work was 60. Among the collected measures, we can list: serum and urinary markers, scores related to aerobic fitness assessment, data from the head-up tilt test with lower body negative pressure (HUT LBNP) test, hematocrit levels, initial weight and height, data from isometric maximum voluntary contraction and muscle fatigue test, data from the posturography, body composition measures from dual-energy x-ray absorptiometry (DEXA) and daily weight. In particular,

- Bone markers consist of urinary N-telopeptide (UNTX), urinary C-telopeptide of type I collagen (UCTX), bone-specific alkaline phosphatase (bAP), procollagen type 1 N-propeptide (PINP), and deoxypyridinoline;

- Aerobic fitness assessment utilizes several key measures, including workload, maximum heart rate (HRmax), maximal oxygen uptake (VO2max), carbon dioxide output (VCO2max), respiratory exchange ratio (RER), and minute ventilation (VE). These metrics provide a comprehensive understanding of an individual's cardiovascular and respiratory capacity during exercise;
- Hematocrit levels are expressed as hematocrit (Hct), plasma volume concentration (PV%), and concentration of total hemoglobin (tHb%);
- From the isometric maximum voluntary contraction evaluation, the knee and ankle range were calculated. At the same time, the difference between the initial and final torque momentum was computed from the muscle fatigue test;
- Posturography measures encompass the mean velocity of the center of force (CoF), the ratio between the path length and the area described by the CoF (Path Length/Area), ellipse eccentricity and angle, and the standard deviation of the anteroposterior movement (CoFx), as well as the mediolateral movement (CoFy). Further measures include peak-to-peak anteroposterior and mediolateral sway, equilibrium scores in both planes, and the dominant frequency at which the CoF oscillates. Posturography was conducted with both eyes open (EO) and closed (EC), the variation (delta, DLT) was calculated as $\Delta = \frac{x_{EC} - x_{EO}}{x_{EC}}$ and employed in the network, where x_{EC} refers to a measure obtained during EC evaluation and x_{EO} refers to a measure obtained during EO evaluation;
- From DEXA scans, the percentage of total mass of bone mineral content (BMC%), the percentage of lean mass (Lean%), and the percentage of fat mass (Fat%) were assessed;
- During head-up tilt test with lower body negative pressure (HUT LBNP) non-invasive arterial blood pressure (ABP) and electrocardiogram (ECG) signals were collected. The series of RR intervals, i.e., the distance between two consecutive R peaks, and the series of systolic, diastolic, and mean arterial pressure values were extracted. Details on this protocol can be found in Linnarsson et al. (2015).

HUT LBNP experiment and cardiovascular signals analysis

The head-up tilt (HUT) lower body negative pressure (LBNP) test is a cardiovascular examination to assess cardiovascular deconditioning and the tolerance to orthostatic stress. It combines HUT, which evaluates cardiovascular responses to passive orthostatic changes using a tilt table, where a vacuum chamber induces a subatmospheric pressure in the lower body (lower body negative pressure, LBNP), promoting blood shifting to the lower extremities and reducing the venous return. After 5 min of baseline, while the subject is positioned supine on the table, the table is tilted to an angle of +80° for at least 15 min. Then, every 3 min, a decreasing pressure of -10 mmHg is applied. The examination continues until the pressure reaches -60 mmHg or until pre-syncopal signs appear. Throughout the duration of the maneuver, ECG and ABP are continuously recorded (Fig. 1). This evaluation was performed both a few days before and at the end of the bed rest. In order to standardize the data across the various studies and to address the heterogeneity of subjects' responses, we used only the first 3 min of baseline measurements and the first 3 min after tilting.

RR interval and systolic blood pressure (SBP)series were cleaned from noise or ectopic beats with an adaptive filter (Wessel et al. 2000), then resampled at 2 Hz, and finally

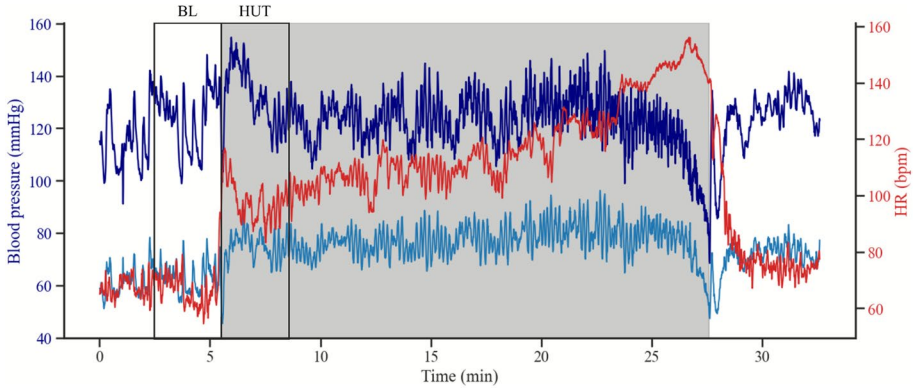

Fig. 1 Example of RR and arterial blood pressure series (i.e., systolic and diastolic blood pressure) recorded during HUT LBNP. The gray area marks the duration of the insult, boxes mark the baseline, i.e., the time period before the start of the experiment, and the first 3 min of tilt

the heart rate and blood pressure variability analysis was performed (Rajendra Acharya et al. 2006). The mean, the standard deviation, and the root mean square deviation were computed for both RR and SBP time series. Successively, the power spectral analysis was performed for both signals. Power spectral analysis is a valuable tool for assessing cardiovascular autonomic regulatory mechanisms (Shaffer et al. 2014). It permits the transformation of time-series data into a frequency domain representation and quantifies different frequency components (bands) that can be linked to specific autonomic influences. Indeed, the sympathetic nervous system's activity is associated with the low frequency (LF) band, 0.04–0.15 Hz, while the high frequency (HF) band, 0.15–0.4 Hz, is associated with parasympathetic activity. Spectral power in LF and HF bands was estimated by integrating the time series' power spectral density (PSD) in these frequency ranges. These quantities were then normalized by the total power (TP) without the very low frequency (VLF: 0–0.04 Hz) component. Additionally, TP was used as an indicator of the total variability (Heart rate variability 1996).

Additionally, the Poincarè and the entropy analyses were performed for RR and SBP time series. Both of them are nonlinear indices related to the signals complexity. The Poincarè plot is a graph in which each RR interval (RR_i) is plotted against the next RR interval (RR_{i+1}), a sort of delay map. The standard deviation along the main diagonal and the anti-diagonal of the obtained cloud of points, SD1 and SD2, respectively, represent the beat-to-beat and longer-term variability. Moreover, the area of the ellipse (S) described by SD1 and SD2 was computed as a measure of total variability (Kamen et al. 1996). Sample entropy (SampEn) and the coefficient of sample entropy (COSEn) measure the degree of randomness and irregularity in a series of data based on the presence of repetitive patterns. They depend on the conditional probability that two similar sequences remain similar for $m + 1$ points, within a tolerance, computed as a percentage of the standard deviation of the signal ($r \cdot \sigma(signal)$) for m points (Lake and Moorman 2011). Furthermore, the sample asymmetry of the RR intervals and SBP time series was computed. This index, initially introduced to detect abnormal patterns in HR variability, such as the presence of decelerations, quantifies the asymmetry of the value distribution, assessing the magnitude of deviations from the median (Kovatchev et al. 2003).

Finally, we also computed the baroreflex sensitivity (BRS) index, which measures how effectively the baroreflex system regulates blood pressure in response to heart rate

fluctuations. It is a key indicator of autonomic nervous system functioning. Briefly, BRS was estimated using an open-loop approach that treats SBP as the input x and RR as the output y of the system. Firstly, it was computed as the average gain of the transfer function $TF(f) = \frac{S_{yx}(f)}{S_x(f)}$ in the LF and HF bands (Robbe et al. 1987) for those frequencies f corresponding to values of coherence, in the normalized cross-spetrum C_{xy}, over 0.5. The BRS index was also computed as the square root of the ratio between RR interval and systolic spectral components $BRS = \sqrt{\frac{S_y(f)}{S_x(f)}}$ in the LF and HF band (Pagani et al. 1988).

Each index I here illustrated was assessed for both the BL and HUT phases; its variation (delta, DLT) $\Delta_I = \frac{I_{HUT} - I_{BL}}{I_{BL}}$ was computed and employed in the network.

Correlation matrices

Once all the indices, i.e., the features, were estimated and retrieved, we reorganized the dataset as the data from the examinations were collected at different time points and intervals. For instance, weight measurements were taken daily, while posturography assessments were conducted two days before and one day after the experiments; bone markers were collected every two to three days. Data collected within the five days after the end of the bed rest protocol were condensed into a time point defined as recovery phase (R). This approach was based on the assumption that measurements remain stable within some days after the conclusion of the bed rest. The missing values in the dataset were imputed using K-nearest neighbors (KNN) imputation. The number of missing values didn't exceed 30%.

To minimize the impact of study heterogeneity on the results, i.e., regarding HDT duration and crossover setups, and considering the small sample size and non-normal distribution of the features, we utilized Spearman partial correlation analysis. This analysis was controlled for three cofactors: the duration of the HDT, the number of trials in the case of crossover studies, and the body mass index (BMI) at the start of the study. Partial correlation, $r_{XY \cdot \mathrm{Z}}$, where $\mathrm{Z} = \{Z_1, Z_2, Z_3\}$ are the controlling variables, measures the degree of association between X and Y features after removing the effect of the controlling variables Z, Practically, this is achieved by calculating the correlation coefficient between the residuals of two linear regressions $X \sim \mathrm{Z}$ and $Y \sim \mathrm{Z}$. This analysis was performed for both time points, BDC and R. Finally, only correlation coefficients with a p-value less than 0.05 were retained, and the absolute values of the coefficients were computed, resulting in two positive-weighted adjacency matrices for BDC and R, respectively. Using the absolute correlation coefficients permits focusing on the strength of the correlations more than the directions. We know that blood pressure and heart rate are related through physiological mechanisms like the arterial baroreflex, as measured by the BRS index; however, the driver of possible changes could be the BP, the HR, or other variables. In this way, the obtained network topology represents the magnitude of physiological interdependence rather than its direction. Future studies could carry out ad hoc analyses, shedding light on the directions of the interactions and how they change after the bed rest.

Network analysis

Graphs are mathematical structures used to model pairwise relations between objects. A graph, also known as a network, is made up of nodes (also called vertices) connected by edges (also called arcs, links, or lines). A distinction is made between undirected graphs, where edges link two nodes symmetrically, and directed graphs, where edges link two nodes asymmetrically. Moreover, the edges may be accompanied by weights, representing the strength of the connection between two different nodes or the flow of information; for this reason, we may distinguish between weighted and unweighted graphs. In our analyses, two undirected weighted networks were constructed using the BDC and R positive-weighted adjacency matrices $W = \{w_{uv}\}$, generated as explained before. We used the Python package *NetworkX* (Hagberg et al. 2008) and Dijkstra's algorithm to find the shortest path in the network.

The average clustering coefficient, global and local efficiencies, and centrality measures were employed to better describe and characterize the network topology, in addition to degree and strength distribution. Furthermore, possible communities were extracted to compare the R and BDC networks and disentangle the key altered relationships.

Clustering coefficient and efficiency

The clustering coefficient measures the degree to which nodes in a graph tend to cluster together. For undirected networks, it is defined as a measure of the number of triangles in a graph, based on a local clustering coefficient for each node. Extensions for weighted graphs also consider the average weight of the triangles. For an undirected unweighted network, the clustering coefficient for the node *u* can be defined as the ratio between the number of triangles connected to node *u* and the number of triples centered around that node. Extension for weighted graphs also considers the average weight of the triangle. It can be assessed as Onnela et al. (2005):

$$c_u = \frac{1}{deg(u)(deg(u)-1)} \sum_{vw} (\hat{w}_{uv}\hat{w}_{uw}\hat{w}_{vw})^{1/3} \tag{1}$$

where $deg(u)$ is the degree of u, i.e. the number of edges it has; $\hat{w}$ are the edge weights normalized by the maximum weight, for example $\hat{w}_{uv} = w_{uv}/w$, where $w = \max(W)$. We evaluate the average clustering coefficient since we aim to achieve a global performance indicator for the entire network.

Efficiency can be defined either as global or local. It provides a measure of the efficiency of information exchanged over the network. High values of global efficiency indicate that short paths are commonly shared among most nodes, ensuring effective long-distance communication. Global efficiency is computed as the average of the reciprocal of the length of the shorter paths, as:

$$E_{global} = \frac{1}{n(n-1)} \sum_{u \neq v} \frac{1}{d(u,v)} \tag{2}$$

where n is the number of nodes and $d(u, v)$ is the length of the shortest path between node u and v. Local efficiency, on the other hand, quantifies how efficiently information is exchanged within local neighborhoods, reflecting the network's resilience to node removal. As suggested in the work of Latora and Marchiori (2001), for each node, we

calculated the global efficiency of the subgraph formed by its neighbors. Then, the local efficiency of the network was obtained by taking the mean of all the nodes.

Centrality measures

Common metrics used to describe a network are centrality indicators, which provide information about node connectivity and importance in the network structure. The degree centrality of a node u is simply the number of edges it has. The value can be normalized by dividing this value by the maximum possible degree $n-1$, where n is the number of nodes in the network. Similarly, in the weighted network, the strength is defined as the sum of the edge weights of the edges incident to that node.

Betweenness centrality measures how much a node serves as a bridge of information flow in the network topology, i.e., it represents the degree to which nodes stand between each other (Brandes 2008). It can be assessed for a node v as:

$$c_B(v) = \sum_{s,t \in V} \frac{\sigma(s,t|v)}{\sigma(s,t)} \tag{3}$$

where V is the set of nodes, $\sigma(s,t)$ is the number of shortest paths from node s to node t, and $\sigma(s,t|v)$ is the number of those paths passing through node v other than s and t.

Closeness centrality reflects the speed of information flow since it is defined as the reciprocal of the average shortest path distance from node v to all other reachable nodes (Freeman 1978):

$$c_C(v) = \frac{n-1}{\sum_{u=1}^{n-1} d(u,v)} \tag{4}$$

where n is the number of nodes and $d(u, v)$ is the shortest path distance between u and v.

Group betweenness centrality is analogous to betweenness centrality but it is calculated for a group of nodes; the same applies to closeness centrality. Group strength, instead, is normalized for the number of nodes to make different group sizes comparable.

Community detection

Community detection algorithms aim to identify possible partitions of the network. In this work, the communities of the generated networks were evaluated through the Louvain method, introduced in 2008 (Blondel et al. 2008). The Louvain method is a greedy optimization method that extracts non-overlapping communities from large networks. The value to be optimized is the modularity Q, defined as a value in the range $[-1, 1]$ that measures the density of edges inside communities compared to edges between communities:

$$Q = \frac{1}{2m} \sum_{uv} w_{uv} - \gamma \frac{k_u k_v}{2m} \delta(c_u, c_v) \tag{5}$$

where m is the number of edges, $W = \{w_{u,v}\}$ is the adjacency matrix, k_u is the degree of the node u, γ is the resolution parameter, and $\delta(c_u, c_v)$ is 1 if the node u and v are in the same community, otherwise is 0. The resolution parameter sets an arbitrary tradeoff between intra-group edges and inter-group edges. We set $\gamma = 1$. This iterative algorithm evaluates community structure, maximizing the highest modularity partition at

each step. The first step consists of assigning a different community to each node. Then, the algorithm evaluates the modularity gain, ΔQ, of removing node u from its community and placing it in the v-community. This procedure is repeated until no further improvement can be achieved. Secondly, a new network is built, aggregating the communities found during the first phase and updating the weights with the sum of weights in the same community. The process is then iterated to obtain a hierarchical community structure, stopping when no further changes are possible or maximum modularity is achieved.

To test the stability and the robustness of the obtained partitions, the analysis was performed 100 times. Then, normalized mutual information (NMI) and variation of information (VI) were evaluated. Similarly, the same metrics were used to evaluate the differences between null model communities and to compare BDC and R partitions. Moreover, for each community, the average intra- and inter-community weights, along with their corresponding ratios, are reported.

Null models and statistical analysis

In network analysis, a null model provides a baseline against which observed network properties can be compared to determine whether these properties are statistically significant or due to chance. The obtained networks, BDC and R, were therefore benchmarked against null models to quantify the significance of their topological properties. The adjacency matrix has a block-wise structure due to the fact that features from the same measurement source are highly correlated, e.g., blood pressure values or the indices related to the heart rate. In contrast, features from different types of measurements tend to be less correlated. To address this, we implemented a block-wise permutation procedure for the adjacency matrices BDC and R, aiming at permuting both inter-group and intra-group edges. Specifically, within the adjacency matrix, edges connecting nodes representing indices from the same type are randomized among themselves. Meanwhile, edges connecting nodes from different domains are randomized across all domains. This allows us to preserve the overall marginal distribution of intra- and inter-group links, while removing specific pairwise patterns, so as to test if the observed structure carries information beyond the block pattern. This procedure was repeated 100 times. Afterward, each graph property was compared against the null distribution. To do this, we calculated a z-score and an empirical p-value (two-sided with $\alpha = 0.05$). Specifically, the p-values were estimated by determining the probability that the observed value exceeded the significance level in the null distribution generated through resampling.

Moreover, to compare the networks (BDC vs R), we've computed the distance between the adjacency matrices using Euclidean, weighted Jaccard, and DeltaCon distances. The distance between adjacency matrices is the simplest method for comparing two graphs and serves as the baseline approach (Tantardini et al. 2019). Given two networks $G_1(V_1, E_1)$ and $G_2(V_2, E_2)$ with adjacency matrix $A_1 = [a^1_{ij}]$ and $A_2 = [a^2_{ij}]$, and identical set of node $V = V_1 = V_2$, we define the Euclidean distance as:

$$d_{EUC}(G_1, G_2) = \sqrt{\sum_{i,j \in V} (a^1_{ij} - a^2_{ij})^2} \tag{6}$$

Weighted Jaccard distance, instead, is the generalization of Jaccard similarity for weighted graphs, defined as:

$$d_{WJAC}(G_1, G_2) = 1 - J_W(A_1, A_2) \tag{7}$$

$$\text{with } J_W(A_1, A_2) = \begin{cases} \frac{\sum_{i,j\in V} min(a^1_{ij}, a^2_{ij})}{\sum_{i,j\in V} max(a^1_{ij}, a^2_{ij})}, & \text{if } \sum_{i,j\in V} max(a^1_{ij}, a^2_{ij}) > 0 \\ 1 & \text{if } \sum_{i,j\in V} max(a^1_{ij}, a^2_{ij}) = 0 \end{cases} \tag{8}$$

On the other hand, DeltaCon (Koutra et al. 2016) is based on the idea of computing the pairwise node affinities in the first graph and comparing them with the ones in the second graph. According to this, for a graph, a similarity matrix is defined as $S = [S_{ij}] = [I + \varepsilon^2 D - \varepsilon A]^{-1}$ where A is the adjacency matrix, D is the degree matrix, and $\varepsilon > 0$ is a small constant capturing the influence between neighboring nodes. This formulation reflects the idea that node i has more influence/affinity to node j if there are many weighted paths from node i to j. Then the distance between G_1 and G_2, for a set of node $V = V_1 = V_2$, is defined using the Matusita distance:

$$d_{DC}(G_1, G_2) = \frac{1}{1 + \sqrt{\sum_{i,j\in V} (\sqrt{s_{1,ij}} - \sqrt{s_{2,ij}})^2}} \tag{9}$$

This gives a similarity value from 0 (completely different) to 1 (identical). Since the constructed networks are nonnegative weighted and bounded, DeltaCon can be easily extended by using the weighted adjacency matrices and the weighted degree matrices. To quantify the contribution of individual nodes to overall network changes, we computed node-level impact scores for each similarity/distance measure. For each metric, the top 10 nodes with the highest impact scores were retained, allowing us to identify nodes most responsible for the observed network differences.

Furthermore, the degree and strength distribution between the obtained networks were compared by means of a two-sided Wilcoxon rank-sum test, while normality is tested using the Shapiro–Wilk test.

Results

The values of all the indices are reported as median, 25th, and 75th percentile in the Table S1, as well as the p-values of the comparison between BDC and R values by means of a paired Wilcoxon signed rank test.

Two networks, representing the baseline (BDC) and the recovery after bed rest (R) conditions, were assessed from the adjacency matrices obtained by considering the significant correlation coefficients among the features. The networks consist of 59 nodes, each of them representing a feature, without the presence of singletons, as shown in Fig. 2. The BDC network visually consists of three main blocks. The first component is associated with posturography-related indices (pink nodes), while the remaining two mainly comprise cardiovascular features. One of these cardiovascular components primarily includes heart rate (HR) and baroreflex indices (purple and orange nodes), whereas the other mainly consists of SBP and hematocrit values (green and olive nodes). Additionally, the R network shows similar results, although the BRS indicators (orange nodes) show some signs of segregation from the other cardiovascular variables.

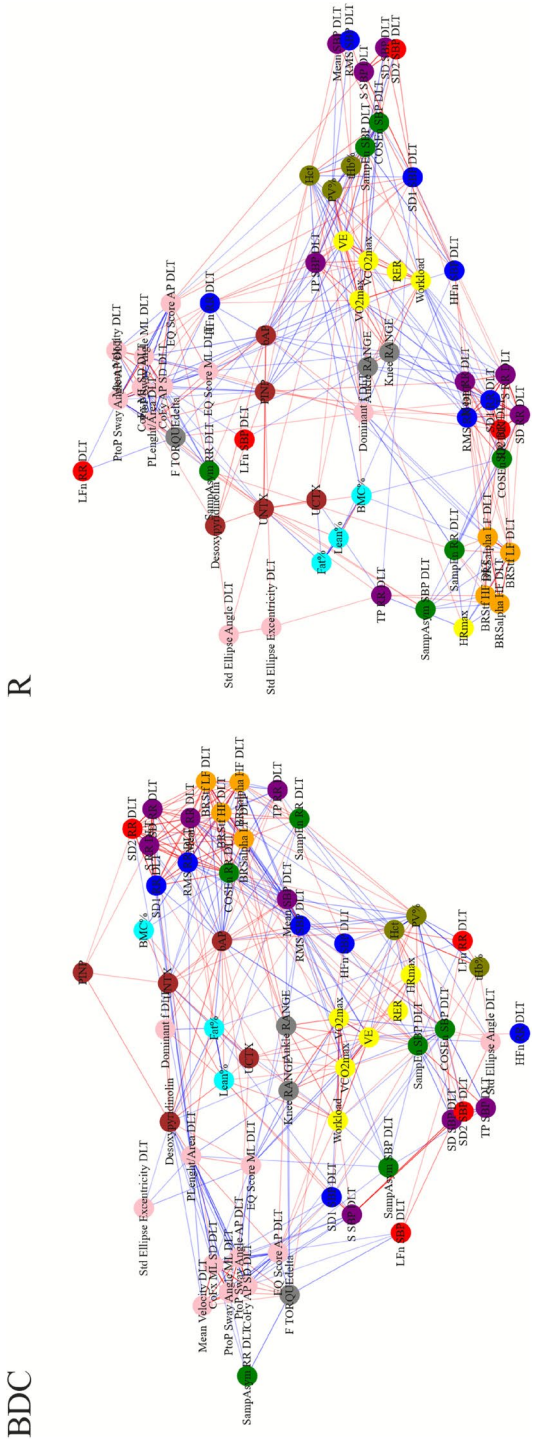

Fig. 2 Topological representation of the obtained network for baseline (BDC, on the left) and recovery (R, on the right). We also indicate the information on the type of correlation: red edges mark a positive correlation between nodes, whereas blue edges mark a negative correlation. Transparency represents the strength of correlation. Parasympathetic features: blue nodes, sympathetic features: red nodes, complexity features: green nodes, total variability: purple nodes, baroreflex indexes: orange nodes, aerobic fitness assessment measures: yellow nodes, bone markers: brown nodes, neurovestibular measures: pink nodes, maximum voluntary contraction measures: grey modes, blood volume indices: olive nodes, body composition scores: cyan nodes

Table 1 Top 10 nodes contributing to network differences according to three similarity/distance measures. Each metric shows the node name and its corresponding impact score. The network-level distance/similarity value is reported below each metric

Euclidean distance		Weighted Jaccard		DeltaCon	
Node	**Score**	**Node**	**Score**	**Node**	**Score**
bAP	0.047	bAP	0.027	bAP	0.043
COSEn RR DLT	0.037	COSEn RR DLT	0.019	COSEn RR DLT	0.031
TP SBP DLT	0.035	TP SBP DLT	0.017	TP SBP DLT	0.030
PV%	0.032	PV%	0.016	Dominant f DLT	0.030
Hct	0.032	Hct	0.016	BRSalpha HF DLT	0.029
BRSalpha HF DLT	0.030	BRSalpha HF DLT	0.016	BRStf HF DLT	0.028
BRStf HF DLT	0.029	BRStf HF DLT	0.016	PINP	0.026
Dominant f DLT	0.026	Dominant f DLT	0.016	RMS SBP DLT	0.026
BRSalpha LF DLT	0.025	Workload	0.015	PV%	0.025
PINP	0.025	VCO2max	0.015	Hct	0.025
distance = 9.47 / Max = 41.36		Similarity = 0.38		Similarity = 0.41	

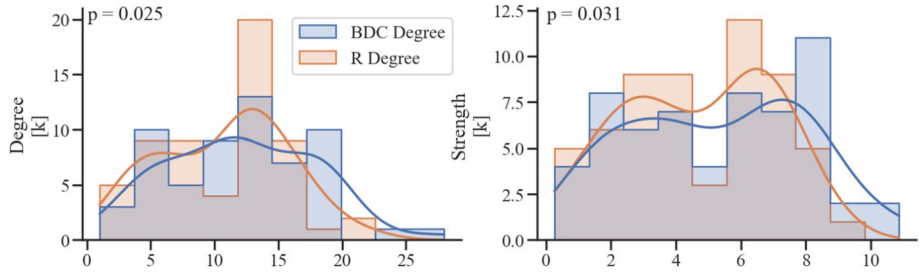

Fig. 3 Histogram of BDC and R networks' degree and strength distribution, with associated two-sided *p*-values employing paired Wilcoxon rank-sum tests

We compared the two correlation-based networks using three complementary metrics: Euclidean distance, weighted Jaccard similarity, and DeltaCon. The Euclidean distance between the networks was 9.46, corresponding to 22.9% of the maximum possible distance (41.36), given the bounded nature of the adjacency matrix, indicating moderate overall changes in edge weights. The weighted Jaccard similarity was 0.38 (dissimilarity 0.62), while DeltaCon yielded a similarity score of 0.41, both of which are consistent with the Euclidean measure and confirm substantial differences between the networks. Node-level impact scores were computed for each metric by summing the contributions of each node's connections (i.e, the rows of the adjacency or affinity matrix, taking advantage of the symmetry of the networks). Across all three metrics, the top contributing nodes were highly consistent, with bAP, COSEn RR DLT, and TP SBP DLT appearing among the top three nodes for all measures. The full ranking of the top 10 nodes for each metric is reported in Table 1, providing a comprehensive view of node-level contributions to network change.

Figure 3 shows the degree and strength distributions (Shapiro–Wilk test for strength: BDC $p = 0.052$, R $p = 0.02$, for degree distributions: BDC $p = 0.1$, R $p = 0.06$). These two distributions are significantly different between the two conditions. This deviation suggests a shift in the topology toward groups of nodes with either high degree and high strength or low degree and low strength, indicating a topological change. Furthermore, the degree and strength are significantly higher in the BDC than in the R network, suggesting a loss of connections.

Table 2 Values of global and local efficiency, average clustering coefficient, weighted clustering coefficient (W. clustering coefficient), average degree, and strength. Moreover, the Z-score and the empirical *p*-value are reported for the comparison with the null models

Metric	BDC	z-score	*p*-value	R	z-score	*p*-value
Global efficiency	0.560	−8.40	0.01	0.533	−6.33	0.01
Local efficiency	0.720	11.45	0.01	0.640	8.91	0.01
Clustering coefficient	0.537	20.34	0.01	0.495	17.10	0.01
W. clustering coefficient	0.243	24.82	0.01	0.236	21.09	0.01
Average degree	12.102	−0.99	n.s	10.712	0.99	n.s
Average strength	5.252	−1.18	n.s	4.710	0.42	n.s

Table 3 Values of centrality measures for each group of features. The features from the head-up tilt (HUT) lower body negative pressure (LBNP) test are split into sub-groups for clarity's sake (cardiovascular, total variability, sympathetic, parasympathetic, baroreflex, and complexity features). * marks those feature groups that have $p < 0.05$ against null models, ** marks those with $p < 0.01$ (empirical *p*-value). Bold values represent the top 2 ranked values in the table. Degree C.: degree centrality; N. Strength: normalized strength

	Betweenness		Closeness		Degree C.		N. Strength	
	BDC	R	BDC	R	BDC	R	BDC	R
Neurovestibular	0.1405**	0.1835**	**2.3656**	2.2289	0.5833	0.5417	**0.4461****	**0.4566**
Blood volume	0.0828	0.1136	1.7781**	1.8727*	0.3214**	0.3214**	0.4199**	0.3945*
Maximum voluntary contraction	0.0318	0.0649	1.7569	1.7987	0.3929	0.3929	0.4009	0.3811
Aerobic fitness assessment	0.1495	0.1107*	2.1125*	2.1017**	0.434**	0.5472*	0.4039	0.4135*
Bone marker	**0.2194**	**0.2334****	2.3395	**2.2812**	**0.6481**	**0.5556**	0.3471	0.3575
Body composition	0.0617	0.0227*	1.771	1.4711	0.2857	0.125	0.3721	**0.484**
Cardiovascular	**0.3118**	**0.2613**	**3.1224**	**3.0103**	**0.8387****	**0.871**	**0.4351****	0.4565*
Total variability	0.0631	0.0949	2.4229	2.1811	0.7059	0.6667	0.4802	0.5098
Sympathetic	0.0283	0.0128	1.899	1.7335	0.4727*	0.3818	0.443	0.4452
Parasympathetic	0.1099	0.1691*	2.206	2.2977	0.6038	0.6981	0.4022**	0.4301*
Baroreflex	0.0303	0.0788	1.7201**	1.7201**	0.3636**	0.2545**	0.4773	0.4737
Complexity	0.1705	0.1201	2.3615	2.1907	0.717	0.717	0.3746**	0.4081**

Global indicators of the network topology, including global and local efficiency, average clustering coefficient, and average degree and strength, are reported in Table 2 along with their associated z-scores and two-sided *p*-values against null distributions. It's worth noting that the average degree and strength cannot be benchmarked against the null model. Since, by construction, they are obtained by permutation, quantities such as average degree and strength are preserved, while topology is not. We can observe a slight decrease in the indices in the R network compared to the BDC network.

Group centrality indicators were computed and reported in Table 3. According to the proposed metrics, i.e., betweenness centrality, closeness centrality, degree centrality, and normalized strength, we observe that bone markers and cardiovascular features are pivotal in both the networks; these features are associated with the highest value for almost all the centrality measures (they are marked in bold in the table). To better disentangle the complex interactions between the autonomic nervous system (ANS) and the different organs and systems measures, the features composing the cardiovascular blocks, i.e., the features of total variability, sympathetic activity, parasympathetic activity, complexity analysis, and baroreflex, were individually investigated. Among them, the features related to the parasympathetic activity and complexity analysis better explain the cardiovascular system's key role in the network.

The centrality measures were also computed for each node; the top 10 variables with the highest score for each measure were reported in Table 4. They were compared to the values obtained from the null model. Bone markers have demonstrated a pivotal role in the network. Compared to null models, bone alkaline phosphatase (bAP) performs superiorly in all centrality indicators. Similarly, cardiovascular-related features emerge as the most significant at baseline, particularly baroreflex indices and COSEn of RR and SBP series, despite a minor role in the R network. This is more pronounced in strength and degree centrality measures, where cardiovascular features were replaced in the top 10 positions mainly by indices derived from aerobic fitness assessments and posturography.

Community detection, using the Louvain method, confirms these findings. To assess the robustness of the detected organization, we evaluated the stability of the Louvain community over 100 repetitions. The resulting partitions were highly consistent across iterations in both conditions, with mean NMI values of 0.94 ± 0.05 for BDC and 0.92 ± 0.06 for R (corresponding VI = 0.04 ± 0.04 and 0.07 ± 0.05, respectively), indicating

Table 4 Values of the centrality measures for the top 10 ranked nodes. * marks those feature groups that have a z-score-associated $p < 0.05$ against null models (two-sided), ** marks those with $p < 0.01$ (empirical p-value)

Betweenness				**Closeness**			
BDC		**R**		**BDC**		**R**	
bAP	0.105**	SD1 SBP DLT	0.097**	bAP	1.893**	bAP	1.797**
Desoxypyridinolin	0.079*	Dominant f DLT	0.092**	RMS SBP DLT	1.827*	SD1 SBP DLT	1.656
VE	0.076**	UNTX	0.078*	Mean SBP DLT	1.784*	Dominant f DLT	1.651*
Hct	0.068	bAP	0.076**	VCO2max	1.770	SampAsym RR DLT	1.627
VCO2max	0.062*	SampAsym RR DLT	0.071**	VE	1.762	PV%	1.625
COSEn SBP DLT	0.057**	PINP	0.071*	Desoxypyridinolin	1.719	Hct	1.625
UCTX	0.042	PV%	0.050	COSEn SBP DLT	1.699	Workload	1.604
RMS SBP DLT	0.042*	TP RR DLT	0.048	Hct	1.686	VE	1.578
COSEn RR DLT	0.041	tHb%	0.047	PV%	1.685	PINP	1.578
SampEn SBP DLT	0.039*	BRStf LF DLT	0.043	SampEn SBP DLT	1.678	HFn RR DLT	1.570
Degree				Strength			
BDC		R		BDC		R	
bAP	0.483**	bAP	0.379**	COSEn RR DLT	10.873*	VO2max	9.033**
COSEn RR DLT	0.397**	Workload	0.345*	bAP	10.675**	Workload	8.132**
COSEn SBP DLT	0.328	VO2max	0.328**	BRSalpha LF DLT	9.453	bAP	8.130**
BRSa1pha LF DLT	0.328	Dominant f DLT	0.293**	RMS RR DLT	8.966	VCO2max	8.084**
BRSalpha HE DLT	0.328	PINP	0.293	Mean RR DLT	8.687	VE	7.780**
Hct	0.328	VCO2max	0.293	BRStf LF DLT	8.478	CoFy AP SD DLT	7.701**
BRStf HF DLT	0.328	VE	0.293	BRSalpha HF DLT	8.424	COSEn SBP DLT	7.288
RMS SBP DLT	0.328	PV%	0.276	BRStf HF DLT	8.329	CoFx ML SD DLT	7.285**
PV%	0.328*	TP SBP DLT	0.276	VCO2max	8.063**	PLenght/ Area DLT	7.165**
VCO2max	0.328**	Hct	0.276	VE	8.019**	PtoP Sway Angle ML DLT	7.010**

stable community detection. However, the similarity between BDC and R partitions was substantially lower (NMI = 0.56, VI = 0.35), indicating a reorganization of the network structure after bed rest. The Louvain method identifies five distinct communities at baseline (BDC network), as shown by the number of nodes in Fig. 4. The first community primarily comprises HR and baroreflex indices from the HUT LBNP test. The second community includes indices related to systolic blood pressure and hematocrit values. The third community consists of posturography measurements. The fourth community mainly consists of indices from aerobic fitness and maximum voluntary contraction tests. Finally, the fifth community connects bone markers with body composition indices. While the connections among these communities have diminished, they can still be partially identified in the R network. However, cardiovascular measurements have become fragmented into various groups. This has resulted in some nodes that are now separated into two distinct communities (4 and 5), each focusing on either heart rate (HR) or baroreflex sensitivity (BRS) indices. In total, there are now six different communities in the R network. The total variability features and baroreflex indices are now separated into different nodes. The indices related to aerobic fitness assessment are now in the first community associated with total variability. All of these communities are illustrated in Fig. 5. To further characterize these changes, we compared the average intra- and inter-community connection strengths. At baseline (BDC), the network exhibited few, relatively large communities with strong internal connections and weaker inter-community coupling. After bed rest (R), the network became more fragmented, with the emergence of smaller communities and a more uneven distribution of internal cohesion. Larger modules lost compactness, exhibiting a lower ratio, whereas smaller clusters became more internally reinforced. This pattern reflects a transition to a fragmented architecture, suggesting a loss of coordination within the system.

Discussions

This study constitutes the first attempt to apply network analyses to bed rest data, elucidating the complex relationships among different physiological systems, all affected by microgravity.

The bed rest is a space flight analog, and it removes the mechanical and hydrostatic stimuli essential for maintaining cardiovascular, musculoskeletal, and neurovestibular tone. These changes not only occur for each physiological system, but also affect their interactions. For example, the loss of gravitational loading, hence a lack of axial forces on the body, causes atrophy and bone demineralization and impairs insulin sensitivity (Heer et al. 2014) The alteration in organ cross-talk is reflected in the topology, as suggested by the significant reduction of the strength and the degree passing from BDC to R, with a consequent reduction of the number of edges (from 357 at BDC to 316 at R). Similarly, the degree and strength distributions shift from a quasi-Gaussian distribution to a bimodal one (Fig. 3), a characteristic of networks with higher node segregation levels, likely related to the presence of disconnected communities as suggested by the increased number of communities and the changes in the intra-/inter- average strength of them. Despite global and local efficiency, the clustering coefficient remains high at recovery, since the correlation networks tend to be fully connected and rich in triangles (Zalesky et al. 2012), a reduction of this average performance (Table 2) can be seen as a change of topology towards a less connected one.

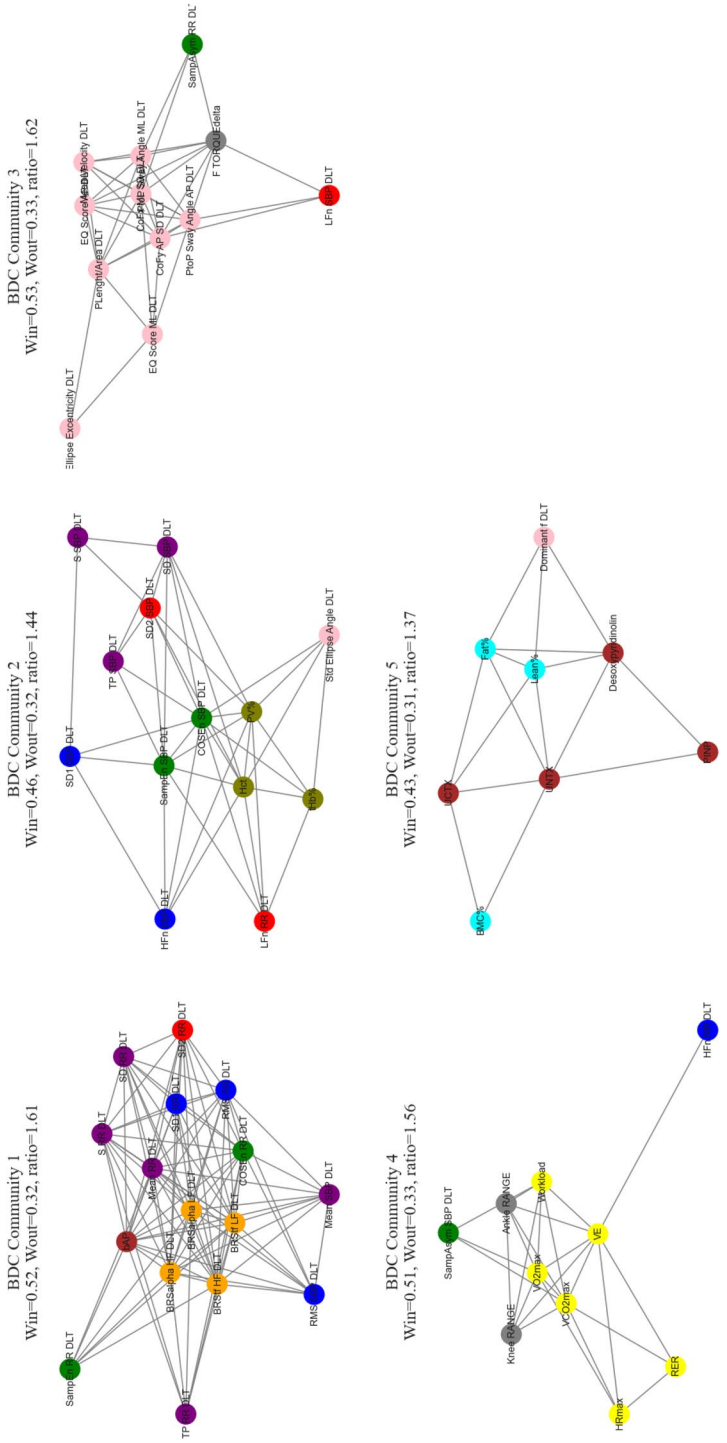

Fig. 4 Representation of the communities extracted through the Louvain method for BDC networks, sorted by number of nodes. Average in- and out-community strength is reported, along with their ratio. Parasympathetic features: blue nodes, sympathetic features: red nodes, complexity features: green nodes, total variability: purple nodes, baroreflex indexes: orange nodes, aerobic fitness assessment measures: yellow nodes, bone markers: brown nodes, neurovestibular and posturography measures: pink nodes, maximum voluntary contraction measures: grey modes, blood volume indices: olive nodes, body composition scores: cyan nodes

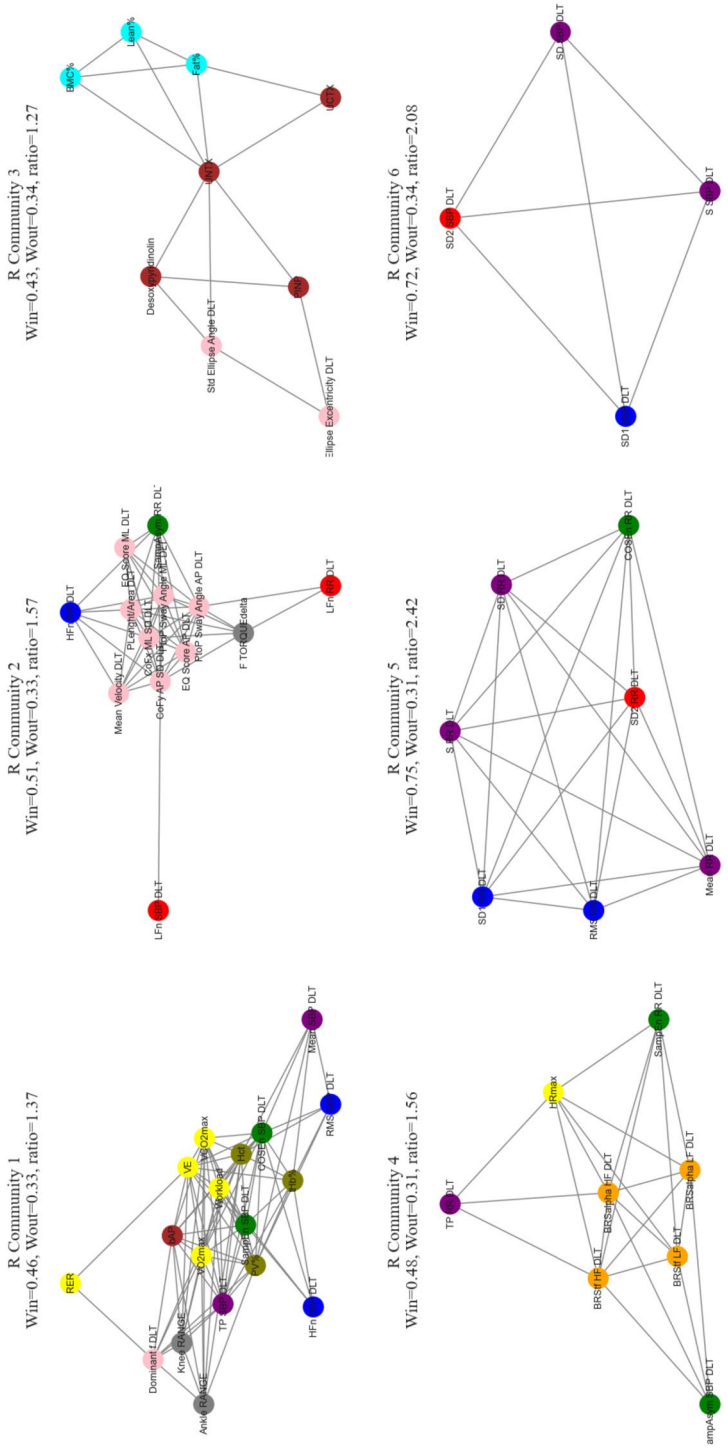

Fig. 5 Representation of the communities extracted through the Louvain method for R networks, sorted by number of nodes. Average in- and out-community strengths are reported, along with their ratio. Parasympathetic features: blue nodes, sympathetic features: red nodes, complexity features: green nodes, total variability: purple nodes, baroreflex indexes: orange nodes, aerobic fitness assessment measures: yellow nodes, bone markers: brown nodes, neurovestibular and posturography measures: pink nodes, maximum voluntary contraction measures: grey modes, blood volume indices: olive nodes, body composition scores: cyan nodes

The cardiovascular deconditioning is largely documented in literature (MendesZambetta et al. 2024). In a microgravity environment, the cardiovascular system experiences significant stress due to the loss of the hydrostatic gradient on blood, creating a fluid volume shift toward the thoracic and central areas. This shift results in an increase in preload and shear stress within the blood vessels, triggering physiological responses mainly driven by the sympathetic branch of the ANS that promotes an increase in HR, hemolysis, reduces plasma volume, and raises blood vessel resistance (Gunga et al. 2016; Hoffmann et al. 2021; Jordan et al. 2022). Additionally, the increased blood flow in the thoracic and central regions may elevate strain on the baroreceptors located in the aortic arch and carotid arteries. This can lead to a shift in the working point of these baroreceptors, impairing the baroreflex and further contributing to cardiovascular decoupling (Convertino 1991; Hargens and Watenpaugh 1996). Our network analysis, particularly the communities extracted through the Louvain method, shows a decoupling of cardiovascular measures. At BDC, the largest community is formed by HR and baroreflex parameters, while SBP-derived measures and plasma indices represent the second-ranked community (Fig. 4). In the R network, the baroreflex forms its own community (community 4), separated from RR indexes, with cardiovascular indexes contaminating other communities and becoming less relevant in the overall representation (Fig. 5). This fragmentation of the two main communities may be related to cardiovascular decoupling and baroreflex impairment. The observed fragmentation of the functional network after bed rest suggests a reduced integration among autonomic and cardiovascular control mechanisms. At baseline, the large, cohesive communities likely represent coordinated regulation between cardiovascular and autonomic components, consistent with an intact baroreflex loop and efficient homeostatic control. However, after prolonged unloading, the breakdown of these large-scale modules and the emergence of smaller, internally dense clusters indicate that information flow becomes more localized, possibly suggesting a partial decoupling between autonomic subsystems. Such reorganization aligns with previous evidence of baroreflex impairment and altered sympathetic parasympathetic balance following exposure to microgravity or head-down bed rest.

The network-level distance analysis confirms a marked topological shift between the two conditions, further supporting findings at the community level. In examining the nodes that contribute most to this distance (Table 1), their profiles closely correlate with changes in centrality measures (Table 3), reinforcing the critical role of cardiovascular factors (particularly those related to complexity, parasympathetic activity, baroreflex response), and bone-related markers in driving this reorganization.

Baroreflex indices have lost their centrality, indicating a reduced role in regulating heart rate and blood pressure. At baseline, these indices function as key hubs within an integrated cardiovascular system, as suggested by their ranking in the top ten for both strength and node degree (Table 3), which reflects efficient baroreflex-mediated coupling. After the bed rest period, their decreased connectivity and strength indicate that the baroreflex loop became functionally isolated, which aligns with impaired feedback between mechanical and autonomic components. Together, these findings emphasize that the observed fragmentation of the network reflects a physiological decoupling of cardiovascular control, a characteristic effect of microgravity-induced deconditioning.

The nodes of bone markers, such as Bone Alkaline Phosphatase (bAP), are connected to nodes related to the neurovestibular system, the muscular system, body composition,

fitness assessment, and cardiovascular measures, although these relationships cannot be fully elucidated. The absence of gravity has been demonstrated to result in a reduction of the musculoskeletal system's requirement to support the body; this phenomenon contributes to the development of osteoporosis and a loss of lean mass (Man et al. 2022). Therefore, the edges connecting nodes related to bone markers, fitness measures, and body composition are in line with these findings. However, the relationships among bone markers, cardiovascular and neurovestibular measures are not straightforward to interpret, as they have never been investigated before. Recent studies on osteoporosis and skeletal pain have uncovered the nervous system's role in bone remodeling (Tomlinson et al. 2020; Elefteriou 2018; Elefteriou et al. 2014). In particular, both sympathetic and parasympathetic nerves were observed in the bone marrow space of long bones, also close to vascular structures, suggesting a possible role of the peripheral nervous system in promoting bone resorption and formation. Studies on knockout mice lacking β adrenergic receptors (Elefteriou et al. 2014) and on the effects of β-blockers (i.e., adrenergic antagonist) (Tomlinson et al. 2020), that reduce the effect of sympathetic activity, show a bone mass increase and a decrease in fracture risk. Similar findings were found about the relationship between vestibular deconditioning and bone remodeling (Vignaux et al. 2015). The vestibular system projects directly onto the central neural circuit, where information is integrated with the autonomic system to support the cardiovascular system in maintaining the orthostatic position and ensuring proper blood perfusion. Experiments on mice with bilateral vestibular lesion show an increase of bone resorption in the lower limbs, probably due to an over-activation of the sympathetic β signaling cascade (Vignaux et al. 2015). Our results suggest a possible interaction between these subsystems, including the role of cardiovascular measures in the network and the loss of centrality at recovery in favor of an increase in the role of the neurovestibular system. We might speculate that pharmacological or non-pharmacological modulation of the ANS, such as vagal stimulation, may represent a new countermeasure that, when combined with others, could help reduce the effects of microgravity on the human body.

This study highlights the feasibility and usefulness of a network-based approach for identifying systemic physiological changes during simulated microgravity. In particular, the findings suggest that the disruption of network integration after bed rest is not uniformly distributed, but is primarily concentrated around nodes representing cardiovascular control and bone metabolism, which may act as early indicators of physiological deconditioning.

Finally, several limitations should be acknowledged. First, the relatively small sample size may affect the generalizability and robustness of these findings. Additionally, the heterogeneity of the included studies (i.e., variations in duration, design, and data acquisition protocols) could introduce residual confounding factors and additional variability in the values. This variability also limits the ability to conduct a longitudinal follow-up. These factors should be taken into account when planning future research.

Conclusion

This study demonstrates the potential of network-based approaches to unravel the complex dynamics of physiological systems under simulated gravity unloading through head down tilt test (HDT). We uncovered subtle yet informative shifts in autonomic regulation across multiple organ systems by integrating multivariate physiological indices into

a correlation-based network. Head-down tilt induced specific topological reconfigurations in physiological networks, particularly in metrics reflecting cardiac and baroreflex deconditioning, that go beyond what traditional univariate analyses reveal, possibly linking with neurovestibular and musculoskeletal systems for the first time. These findings open new avenues for targeting autonomic dysregulation through vagal nerve stimulation and beta-adrenergic blockade interventions. These interventions, combined with another countermeasure, may help mitigate the effects of microgravity in space missions.

Future studies should validate these insights in longer-duration analogs and actual spaceflight, and explore integration with additional omics or imaging data to characterize individual responsiveness, including new points of view in the network.

Supplementary Information

The online version contains supplementary material available at https://doi.org/10.1007/s41109-026-00773-8.

Supplementary Material 1.

Acknowledgements
The study was performed using data provided by the European Space Agency (ESA) for the project "DAYSTAR: Bedrest as an experimental condition to disentangle the interactions between the autonomic nervous system (ANS), sleep, mental health, metabolism, and bone remodeling," which was awarded under the call "Retrospective Analysis of Bedrest Core Data: a SciSpacE Announcement of Opportunity" (AO-2023-BedrestCoreData).

Author contributions
R.A. has analyzed the data, drafted, and revised the manuscript. M.F. has supervised the analyses, drafted, and revised the manuscript. A.C., G.D.R., E.T., and N.M. revised the manuscript. All authors read and approved the final manuscript.

Funding
Research fellowship of Riccardo Asnaghi is funded by the National Plan for NRRP Complementary Investments (PNC, established with the decree-law 6 May 2021, n. 59, converted by law n. 101 of 2021) in the call for the funding of research initiatives for technologies and innovative trajectories in the health and care sectors (Directorial Decree n. 931 of 06-06-2022) - project n. PNC0000003 - AdvaNced Technologies for Human-centrEd Medicine (project acronym: ANTHEM). This work reflects only the authors' views and opinions, neither the Ministry for University and Research nor the European Commission can be considered responsible for them.

Data availability
The data adopted in this study are propriety of the European Space Agency (ESA).They comes from several bed rest study, access to specific data sets may require contacting the ESA Human Research Office or the study authors directly.

Declarations

Competing interests
The authors declare that they have no conflict of interest.

Received: 4 June 2025 / Accepted: 14 January 2026
Published online: 05 February 2026

References

Arc-Chagnaud C, Py G, Fovet T, Roumanille R, Demangel R, Pagano AF, Delobel P, Blanc S, Jasmin BJ, Blottner D, Salanova M, Gomez-Cabrera M-C, Viña J, Brioche T, Chopard A (2020) Evaluation of an antioxidant and anti-inflammatory cocktail against human hypoactivity-induced skeletal muscle deconditioning. Front Physiol 11:71. https://doi.org/10.3389/fphys.2020.00071

Bashan A, Bartsch RP, Kantelhardt JW, Havlin S, Ivanov PC (2012) Network physiology reveals relations between network topology and physiological function. Nat Commun 3(1):702. https://doi.org/10.1038/ncomms1705

Blondel VD, Guillaume J-L, Lambiotte R, Lefebvre E (2008) Fast unfolding of communities in large networks. J Stat Mech 2008(10):10008. https://doi.org/10.1088/1742-5468/2008/10/P10008

Blottner D, Bosutti A, Degens H, Schiffl G, Gutsmann M, Buehlmeier J, Rittweger J, Ganse B, Heer M, Salanova M (2014) Whey protein plus bicarbonate supplement has little effects on structural atrophy and proteolysis marker immunopatterns in skeletal muscle disuse during 21 days of bed rest. J Musculoskelet Neuronal Interact 14(4):432–444

Brandes U (2008) On variants of shortest-path betweenness centrality and their generic computation. Soc Netw 30(2):136–145. https://doi.org/10.1016/j.socnet.2007.11.001

Convertino VA (1991) Carotid-cardiac baroreflex: relation with orthostatic hypotension following simulated microgravity and implications for development of countermeasures. Acta Astronautica 23:9–17. https://doi.org/10.1016/0094-5765(91)90093-K

Elefteriou F (2018) Impact of the autonomic nervous system on the skeleton. Physiol Rev 98(3):1083–1112. https://doi.org/10.1152/physrev.00014.2017
Elefteriou F, Campbell P, Ma Y (2014) Control of bone remodeling by the peripheral sympathetic nervous system. Calcif Tissue Int 94(1):140–151. https://doi.org/10.1007/s00223-013-9752-4
Freeman LC (1978) Centrality in social networks conceptual clarification. Soc Netw 1(3):215–239. https://doi.org/10.1016/0378-8733(78)90021-7
Frett T, Green DA, Mulder E, Noppe A, Arz M, Pustowalow W, Petrat G, Tegtbur U, Jordan J (2020) Tolerability of daily intermittent or continuous short-arm centrifugation during 60-day 6o head down bed rest (AGBRESA study). PLoS ONE 15(9):0239228. https://doi.org/10.1371/journal.pone.0239228
Guinet P, MacNamara JP, Berry M, Larcher F, Bareille M-P, Custaud M-A, Pavy-Le Traon A, Levine BD, Navasiolava N (2020) MNX (medium duration nutrition and resistance-vibration exercise) bed-rest: effect of resistance vibration exercise alone or combined with whey protein supplementation on cardiovascular system in 21-day head-down bed rest. Front Physiol. https://doi.org/10.3389/fphys.2020.00812
Gunga H-C, Ahlefeld VWV, Appell Coriolano H-J, Werner A, Hoffmann U (2016) Cardiovascular system, red blood cells, and oxygen transport in microgravity. SpringerBriefs Sp Life Sci. https://doi.org/10.1007/978-3-319-33226-0
Hagberg AA, Schult DA, Swart PJ (2008) Exploring network structure, dynamics, and function using NetworkX, pp 11–15. https://doi.org/10.25080/TCWV9851.https://doi.curvenote.com/10.25080/TCWV9851 Accessed 2025-05-09
Hargens AR, Watenpaugh DE (1996) Cardiovascular adaptation to spaceflight. Med Sci Sports Exerc 28(8):977
Heart rate variability (1996) standards of measurement, physiological interpretation and clinical use. Task force of the European society of cardiology and the north American society of pacing and electrophysiology. Circulation 93(5):1043–1065
Heer M, Baecker N, Wnendt S, Fischer A, Biolo G, Frings-Meuthen P (2014) How fast is recovery of impaired glucose tolerance after 21-day bed rest (NUC study) in healthy adults? Sci World J 2014:803083. https://doi.org/10.1155/2014/803083
Hoffmann F, Rabineau J, Mehrkens D, Gerlach DA, Moestl S, Johannes BW, Caiani EG, Migeotte PF, Jordan J, Tank J (2021) Cardiac adaptations to 60 day head-down-tilt bed rest deconditioning. findings from the AGBRESA study. ESC Heart Failure 8(1):729–744. https://doi.org/10.1002/ehf2.13103
Hoffmann B, Dehkordi P, Khosrow-Khavar F, Goswami N, Blaber AP, Tavakolian K (2022) Mechanical deconditioning of the heart due to long-term bed rest as observed on seismocardiogram morphology. NPJ Microgravity 8(1):25. https://doi.org/10.1038/s41526-022-00206-7
Jordan J, Limper U, Tank J (2022) Cardiovascular autonomic nervous system responses and orthostatic intolerance in astronauts and their relevance in daily medicine. Neurol Sci 43(5):3039–3051. https://doi.org/10.1007/s10072-022-05963-7
Kamen PW, Krum H, Tonkin AM (1996) Poincaré plot of heart rate variability allows quantitative display of parasympathetic nervous activity in humans. Clin Sci (Lond) 91(2):201–208. https://doi.org/10.1042/cs0910201
Klimek P, Aichberger S, Thurner S (2016) Disentangling genetic and environmental risk factors for individual diseases from multiplex comorbidity networks. Sci Rep 6:39658. https://doi.org/10.1038/srep39658
Koutra D, Shah N, Vogelstein JT, Gallagher B, Faloutsos C (2016) DeltaCon: principled massive-graph similarity function with attribution. ACM Trans Knowl Discov Data 10(3):28–12843. https://doi.org/10.1145/2824443
Kovatchev BP, Farhy LS, Cao H, Griffin MP, Lake DE, Moorman JR (2003) Sample asymmetry analysis of heart rate characteristics with application to neonatal sepsis and systemic inflammatory response syndrome. Pediatr Res 54(6):892–898. https://doi.org/10.1203/01.PDR.0000088074.97781.4F
Kramer A, Kümmel J, Mulder E, Gollhofer A, Frings-Meuthen P, Gruber M (2017) High-intensity jump training is tolerated during 60 days of bed rest and is very effective in preserving leg power and lean body mass: An overview of the cologne RSL study. PLoS ONE 12(1):0169793. https://doi.org/10.1371/journal.pone.0169793
Lake DE, Moorman JR (2011) Accurate estimation of entropy in very short physiological time series: the problem of atrial fibrillation detection in implanted ventricular devices. Am J Physiol Heart Circ Physiol 300(1):319–325. https://doi.org/10.1152/ajpheart.00561.2010
Latora V, Marchiori M (2001) Efficient behavior of small-world networks. Phys Rev Lett 87(19):198701. https://doi.org/10.1103/PhysRevLett.87.198701
Linnarsson D, Hughson RL, Fraser KS, Clément G, Karlsson LL, Mulder E, Paloski WH, Rittweger J, Wuyts FL, Zange J (2015) Effects of an artificial gravity countermeasure on orthostatic tolerance, blood volumes and aerobic power after short-term bed rest (BR-AG1). J Appl Physiol 118(1):29–35. https://doi.org/10.1152/japplphysiol.00061.2014
Man J, Graham T, Squires-Donelly G, Laslett AL (2022) The effects of microgravity on bone structure and function. NPJ Microgravity 8(1):1–15. https://doi.org/10.1038/s41526-022-00194-8
MendesZambetta R, Signini EDF, Ocamoto GN, Catai AM, Uliam NR, Santarnecchi E, Russo TL (2024) Effects of weightlessness on the cardiovascular system: a systematic review and meta-analysis. Front Physiol 15:1438089. https://doi.org/10.3389/fphys.2024.1438089
Morabito A, De Simone G, Magri S, Mongelli A, Ferrario M, Pastorelli R, Mariotti C, Taroni F, Diomede L, Schiarea S, Brunelli L (2025) Correlation networks to uncover changes in protein relationships in spinocerebellar ataxia type 2 and cerebellar multiple system atrophy. J Proteome Res 24(7):3379–3388. https://doi.org/10.1021/acs.jproteome.5c00081
Onnela J-P, Saramäki J, Kertész J, Kaski K (2005) Intensity and coherence of motifs in weighted complex networks. Phys Rev E 71(6):065103. https://doi.org/10.1103/PhysRevE.71.065103
Pagani M, Somers V, Furlan R, Dell'Orto S, Conway J, Baselli G, Cerutti S, Sleight P, Malliani A (1988) Changes in autonomic regulation induced by physical training in mild hypertension. Hypertension 12(6):600–610. https://doi.org/10.1161/01.HYP.12.6.600
Rajendra Acharya U, Paul Joseph K, Kannathal N, Lim CM, Suri JS (2006) Heart rate variability: a review. Med Bio Eng Comput 44(12):1031–1051. https://doi.org/10.1007/s11517-006-0119-0
Rittweger J, Bareille M-P, Clément G, Linnarsson D, Paloski WH, Wuyts F, Zange J, Angerer O (2015) Short-arm centrifugation as a partially effective musculoskeletal countermeasure during 5-day head-down tilt bed rest—results from the BRAG1 study. Eur J Appl Physiol 115(6):1233–1244. https://doi.org/10.1007/s00421-015-3120-1
Robbe HW, Mulder LJ, Rüddel H, Langewitz WA, Veldman JB, Mulder G (1987) Assessment of baroreceptor reflex sensitivity by means of spectral analysis. Hypertension 10(5):538–543. https://doi.org/10.1161/01.hyp.10.5.538
Ruyters G, Braun M, Stang KM (2021) Breakthroughs in space life science research: from apollo 16 to the iss. SpringerBriefs Space Life Sci Springer. https://doi.org/10.1007/978-3-030-74022-1

Shaffer F, McCraty R, Zerr CL (2014) A healthy heart is not a metronome: an integrative review of the heart's anatomy and heart rate variability. Front Psychol 5:1040. https://doi.org/10.3389/fpsyg.2014.01040
Tantardini M, Ieva F, Tajoli L, Piccardi C (2019) Comparing methods for comparing networks. Sci Rep 9(1):17557. https://doi.org/10.1038/s41598-019-53708-y
Tomlinson RE, Christiansen BA, Giannone AA, Genetos DC (2020) The role of nerves in skeletal development, adaptation, and aging. Front Endocrinol. https://doi.org/10.3389/fendo.2020.00646
Váša F, Mišić B (2022) Null models in network neuroscience. Nat Rev Neurosci 23(8):493–504. https://doi.org/10.1038/s41583-022-00601-9
Vernice NA, Meydan C, Afshinnekoo E, Mason CE (2020) Long-term spaceflight and the cardiovascular system. Precis Clinic Med 3(4):284–291. https://doi.org/10.1093/pcmedi/pbaa022
Vernikos J (1996) Human physiology in space. BioEssays. 18(12):1029–1037. https://doi.org/10.1002/bies.950181215
Vignaux G, Ndong JD, Perrien DS, Elefteriou F (2015) Inner ear vestibular signals regulate bone remodeling via the sympathetic nervous system. J Bone Miner Res 30(6):1103–1111. https://doi.org/10.1002/jbmr.2426
Wessel N, Voss A, Malberg H, Ziehmann C, Voss HU, Schirdewan A, Meyerfeldt U, Kurths J (2000) Nonlinear analysis of complex phenomena in cardiological data. Herzschrittmachertherapie und Elektrophysiologie 11(3):159–173. https://doi.org/10.1007/s003990070035
Zalesky A, Fornito A, Bullmore E (2012) On the use of correlation as a measure of network connectivity. Neuroimage 60(4):2096–2106. https://doi.org/10.1016/j.neuroimage.2012.02.001

Publisher's Note